Dual-Energy CT for Pediatric Thoracic Imaging: A Review

Jordan B. Rapp, MD[1], David M. Biko, MD[1], Marilyn J. Siegel, MD[2]

Pediatric Imaging · Review

Keywords

CT, dual-energy CT, pediatrics, radiation dose

Submitted: Feb 26, 2023
Revision requested: Mar 15, 2023
Revision received: Apr 18, 2023
Accepted: May 2, 2023
First published online: May 17, 2023
Version of record: Aug 16, 2023

M. J. Siegel receives lecture honoraria from Siemens Healthineers. The remaining authors declare that there are no other disclosures relevant to the subject matter of this article.

doi.org/10.2214/AJR.23.29244

AJR 2023; 221:526–538

ISSN-L 0361–803X/23/2214–526

Dual-energy CT has expanded the potential of thoracic imaging in both children and adults. Data processing allows material- and energy-specific reconstructions, which improve material differentiation and tissue characterization compared with single-energy CT. Material-specific reconstructions include iodine, virtual unenhanced, perfusion blood volume, and lung vessel images, which can improve assessment of vascular, mediastinal, and parenchymal abnormalities. The energy-specific reconstruction algorithm allows virtual monoenergetic reconstructions, including low-energy images to increase iodine conspicuity and high-energy images to reduce beam-hardening and metal artifacts. This review highlights dual-energy CT principles, hardware, and postprocessing algorithms; the clinical applications of dual-energy CT; and the potential benefits of photon counting (the most recently introduced iteration of spectral imaging) in pediatric thoracic imaging.

Conventional, or single-energy, CT provides information on the x-ray attenuation coefficient (measured as Hounsfield units) at a single-energy level (expressed as kilovoltage). Single-energy CT has limited ability to differentiate materials, particularly iodine and calcium (bone), which can have similar attenuation in Hounsfield units depending on the concentrations of the two elements [1–5]. Dual-energy CT, also known as spectral CT, enables near-simultaneous acquisition of CT images at two kilovoltage peaks, which yields additional information about tissue composition and allows differentiation of tissues with similar attenuation.

Dual-energy and photon-counting detector CT offer a variety of available options for spectral imaging of the chest. In this article, we review the basic principles of dual-energy CT as well as the various types of dual-energy CT scanners and their benefits and limitations. We elaborate on the available postprocessing algorithms and detail their role in the assessment of various disorders, many of which are unique to children and require special consideration. These include congenital lung lesions, chronic lung disease of prematurity, congenital chest masses, and childhood-related malignancies. Additional entities and uses more common in children, such as hereditary hemorrhagic telangiectasia, pulmonary artery and pulmonary vein stenosis, and scoliosis-related hardware, are described. Certain pathologies that occur more frequently in adults, such as pulmonary hypertension and pulmonary embolism, are also discussed given their relevance to pediatric application of dual-energy CT.

Principles of Dual-Energy CT

In CT, tissue attenuation occurs primarily through a combination of Compton scattering and photoelectric absorption. Compton scattering dominates at higher energies and primarily depends on the electron density of materials. Photoelectron absorption dominates at lower energies and is linked to both the atomic number (Z) and the mass density of materials (ρ) and tissues. The likelihood of a photoelectron interaction increases in materials with high atomic numbers, particularly iodine ($Z = 53$) and calcium ($Z = 20$). The probability of a photoelectron effect decreases in compounds that comprise materials with a low atomic number, including soft tissue, water, and fat (for hydrogen, $Z = 1$; for carbon, $Z = 6$; for nitrogen, $Z = 7$; for oxygen, $Z = 8$).

[1]Department of Radiology, Children's Hospital of Philadelphia, Philadelphia, PA.

[2]Edward Mallinckrodt Institute of Radiology, Washington University School of Medicine, 510 S Kingshighway Blvd, St. Louis, MO 63110. Address correspondence to M. J. Siegel (siegelm@wustl.edu).

Dual-Energy CT Scanners

Single-Source Scanners

An array of single-source hardware systems are available for acquiring dual-energy images. Single-source rapid-kilovoltage-switching dual-energy CT uses a single x-ray tube that rapidly alternates between low (80 kV) and high (140 kV) energies and a single detector that quickly captures the data from both energies. Dual-layer–detector dual-energy CT uses a single x-ray beam operating at 120 or 140 kV and a single detector made of two layers: a superficial layer that absorbs lower-energy x-ray photons and a deeper layer that absorbs higher-energy photons [6]. A benefit of dual-layer scanners is the ability to select the dual-energy method after scanning, as spectral data are always available. Twin-beam dual-energy CT uses a high-energy tube operating at 120 kV and a filter that splits the beam into high- and low-energy spectra before it reaches the patient [7, 8].

Dose reduction capabilities, such as automated tube current modulation, are available on all single-source systems except for rapid-kilovoltage-switching systems. In the latter system, the exposure-time ratio increases for the 80-kV acquisition and decreases for the 140-kV acquisition to reduce radiation exposure [9]. Single-source systems are not limited in terms of the FOV of the dual-energy portion of the image, although dual-source systems are limited in terms of this FOV (as described in the next section) because a different detector size is used for each tube.

Dual-Source Scanners

Second- and third-generation dual-source dual-energy CT scanners use two x-ray tubes that operate independently at low and high energies and two detectors that simultaneously acquire and process the dual-energy data. The second-generation scanner operates at 80 and 140 kV and has an FOV of 50 and 33 cm for the low- and high-energy tubes, respectively. The third-generation scanner operates at 70 and 150 kV and has an FOV of 50 and 35 cm for the low- and high-energy tubes, respectively. The gantry rotation time is decreased to 0.25 second from 0.28 second, allowing faster speed.

Automated tube current modulation is available for dose reduction. In addition, dual-source CT scanners have a tin filter in front of the high-kilovoltage x-ray tube to attenuate low-energy photons, further decreasing radiation exposure and increasing spectral separation] [9–11]. Although dual-source CT has the added benefit of scanning at an ultrahigh pitch of greater than 3, a limitation of the use of dual energy in dual-source systems is the inability to scan at such a pitch. In dual-energy mode, the pitch is limited to 1.5, similar to the pitch used for a single-source scanner. Thus, the scanning time cannot be decreased relative to a dual-source single-energy ultrahigh-pitch technique, restricting the ability to reduce patient motion [12]. The inability to use ECG gating may limit use of dual-source dual-energy CT in cardiac or vascular evaluations.

Photon-Counting Detector CT

Photon-counting detector technology is the latest iteration of CT hardware [13, 14]. Conventional CT uses a two-step process in which x-rays are converted to light via a ceramic scintillator and that light is converted to an electronic signal by photodiodes. Photon-counting detector CT improves on conventional CT because it uses a one-step process to convert x-rays directly to electrons by means of a crystal semiconductor. In this process, the detector separates the photons directly into two to eight bins on the basis of the energy, allowing acquisition of different energy levels from a single source [14]. Photon-counting detector CT improves dose efficiency compared with conventional CT, related to the use of smaller detector collimation (0.4 mm), elimination of reflective septa within the detectors, and elimination of electronic noise [14]. Other benefits of this technology are the improved spatial resolution and multienergy data acquisition built into each scan. Photon-counting detector CT also allows high-pitch imaging and gated cardiac CT.

Highlights

- *Dual-energy CT with use of material-specific images allows pulmonary vascular flow and lung perfusion assessment, tumor characterization, and treatment response evaluation.*
- *Dual-energy CT with use of energy-specific images allows improved intravascular contrast at low energies and reduced beam-hardening and metal artifacts at high energies.*
- *Dual-energy CT can be performed with radiation exposures less than or similar to those of single-energy CT, which is of particular importance in children.*

Dual-Energy CT Reconstruction Algorithms

Second- and third-generation dual-source scanners generate three routine image sets at the console that are available for immediate diagnostic interpretation, including low-energy (70 or 80 kV), high-energy (140 or 150 kV), and mixed (or blended) image sets [9, 15]. The mixed image set typically comprises 50% of the data from each of the low- and high-energy image sets and is equivalent to a 120-kV image. The mixed images, as well as the 70- or 80-kV images, are sent to the PACS for interpretation. The high-energy (140 or 150 kV) images typically are not sent to the PACS for interpretation owing to the poorer CNR. In comparison, single-source scanners generate either a 120- or 140-kV image at the console, which is sent to the PACS for interpretation.

Additional reconstructions include material-specific images and energy-specific (also referred to as virtual monoenergetic) images [9, 15, 16]. On single- and dual-source scanners and photon-counting detector CT scanners, material-specific images include iodine and virtual unenhanced images (Fig. 1). Dual-source scanners have additional material-specific algorithms, including algorithms for imaging of perfused blood volume and lung vessels (Fig. 2). These reconstructions may be configured at the time of scanning and sent directly to the PACS for interpretation, or they may be created later at a remote workstation. The software also allows measurement of the quantity of iodine within a given tissue (expressed as milligrams per milliliter), using ROIs or lung segmentation tools.

Material-Specific Images

Iodine Images

Iodine images display the distribution of iodine in lung and soft-tissue structures and allow both qualitative and quantitative assessments of iodine content. The iodine content can be dis-

played either as a pure iodine map or as an iodine overlay or fusion image (i.e., iodine superimposed on a CT image) [1]. Iodine images play a role in assessing the presence and pattern of distribution of contrast material in mediastinal masses, lung nodules, and adenopathy; this information can help characterize lesions and monitor treatment response [17].

Virtual Unenhanced Images

Virtual unenhanced images are acquired by subtracting the contrast material out of the iodine image. This image set is helpful in determining whether high-radiodensity material seen on routine anatomic reconstructions represents true contrast material or other materials, such as calcium or blood [18]. The image set also has the potential to reduce radiation by eliminating the need for a true unenhanced dataset; elimination of this acquisition is especially beneficial for imaging of the pediatric population.

Perfused Blood Volume Images

Perfused blood volume (PBV) is designed to visualize and quantify iodine uptake in the lung parenchyma (Fig. 2). This image set reflects iodine attenuation in lung parenchyma at a single time point and is a surrogate for lung perfusion [3]. Analysis is restricted to the lung parenchyma using a threshold-based function based on CT attenuation. In adolescents and adults, the maximum CT attenuation value is –600 HU. In younger children, the maximum attenuation value increases to –200 to –300 HU (referred to as dense lung setting), to account for the normal higher lung attenuation in this population [19]. Structures outside of this attenuation range are not included in the PBV calculation. On standard PBV images, normal lung perfusion is homogeneous and can be color-coded reddish orange. Other PBV schemes are available, such that lung perfusion can be displayed in multiple colors depending on user preference. PBV imaging has a role in evaluating perfusion in pulmonary vascular and parenchymal diseases. Iodine concentrations can be measured using vendor-specific software that allows quantifiable comparison between lobes and serial examinations.

Pulmonary Vessel Imaging

Pulmonary vessel imaging, available on dual-source scanners, shows the amount of iodine in vascular structures as an indicator of flow. Pulmonary vessels with high flow are color-coded blue, and those with slower flow are color-coded red. Slower flow can indicate later arrival of contrast material in a vessel due to obstruction or dilution effect of collaterals. This algorithm complements PBV images and is useful in the assessment of vascular and parenchymal diseases.

Virtual Monoenergetic Images

Virtual monoenergetic images simulate the attenuation (expressed as Hounsfield units) of an image acquired at a single energy value, allowing extrapolation of energies as low as 40 keV and as high as 200 keV. Low–kiloelectron voltage images (40–50 keV) use an energy close to the K-edge of iodine (32 keV) and are useful to increase the conspicuity of contrast material [9, 15, 16] (Fig. 3). These images also can allow use of smaller volumes of contrast material and lower injection rates [20]. High–kiloelectron voltage images (100–150 keV) decrease noise and are useful in reducing beam-hardening artifacts related to dense intravascular contrast material and metal implants, such as those associated with spinal instrumentation [21] (Fig. 4).

Radiation Exposure

Radiation exposure from diagnostic imaging in children is an important consideration because of concerns about the potential risk for radiation-induced carcinogenesis. In pediatric chest CT, clinical studies of dual-source CT scanners have reported that doses are equal to or less than those of single-energy CT when traditional dose reduction techniques are used [9, 22–24].

Explanations for the reduced dose on the dual-source system are as follows: the addition of tin filtration, which absorbs unnecessary low-energy photons in dual-source CT scanners; use of virtual noncontrast images, which may obviate acquisition of true noncontrast images; and improvements in iterative reconstruction techniques and detector efficiency, particularly when a photon-counting detector system is used.

Dual-Energy CT in Pulmonary Vascular Imaging

Pulmonary Embolism

Among children, the prevalence of pulmonary thromboembolism on CTA is approximately 16% [25, 26]. Although pulmonary thromboembolism shows many of the same imaging findings in adult and pediatric patients, the challenges of using CTA to diagnose pulmonary emboli in children include difficulty in visualizing small pulmonary emboli in small patients and difficulty in obtaining optimal pulmonary arterial opacification in small patients. Low–kiloelectron voltage monoenergetic (40–50 keV) images can improve enhancement of the pulmonary arteries, potentially salvaging an examination with suboptimal enhancement. Vessel and PBV images can improve both the detectability of small endoluminal thrombi and the effect of such thrombi on lung perfusion. In a study comparing average-weighted 120-kV images and perfusion images in the detection of pulmonary embolus in 32 children with nephrotic syndrome, the authors reported that PBV images improved detection of segmental and subsegmental pulmonary emboli, although the difference was not statistically significant [23].

Material-specific PBV and pulmonary vessel images provide information about lung perfusion and vessel patency [9, 15, 23, 27–30]. On PBV images, perfusion defects associated with occlusive pulmonary thromboembolism manifest as peripheral wedge-shaped areas of nonenhancing parenchyma (Fig. 5). Occlusive emboli are more likely than nonocclusive emboli to show perfusion defects [27]. Thrombosed pulmonary arteries are color-coded red, reflecting diminished or absent flow (Fig. 5). The lung vessel algorithm, a currently available postprocessing tool, can improve detection of small emboli in segmental and subsegmental pulmonary arteries in comparison with conventional CTA [30, 31], although the clinical significance of this finding is uncertain [31].

Pulmonary Hypertension

In children, pulmonary hypertension is usually idiopathic or due to high-flow congenital heart disease and, less often, embolic disease. Material-specific images are useful to detect subtle decreases in parenchymal perfusion and pulmonary flow, allowing diagnosis of pulmonary hypertension when conventional CTA is

normal. These images also can be used in treatment monitoring. The parenchymal abnormalities on PBV images are large, peripheral, and segmental in embolic hypertension, but they tend to be smaller, nonsegmental, and patchy in nonembolic pulmonary hypertension [32, 33] (Fig. 6). Defects are more likely to be seen in severe disease than in mild disease. Restricted arterial flow (color-coded red) can be seen on pulmonary vessel images.

Arteriovenous Malformations

CTA has played an increasing role in the identification and description of arteriovenous malformations [34]. Early experience has suggested that PBV images and lung vessel images are useful for increasing the conspicuity of small arteriovenous malformations and their nidi, for example in young patients with hereditary hemorrhagic telangiectasia [9, 30]. In addition, initial experience suggests that dual-energy CT can be used to evaluate the success of embolization [9] (Fig. 7). Larger series are required to define the value of dual-energy CT in the evaluation and management of arteriovenous malformations.

Vascular Abnormalities

Dual-energy material-specific images can add information to conventional CTA in the evaluation of lung perfusion and pulmonary artery flow in patients with congenital heart diseases associated with hypoplastic or absent pulmonary arteries [9] and in preoperative planning for pulmonary artery reconstruction [35]. Assessment of lung perfusion in pulmonary venous obstruction is another indication for PBV imaging by dual-energy CT (Fig. 8). Other studies have shown a role of dual-energy CT in the evaluation of cyanotic congenital heart disease, by using PBV images as a surrogate for lung perfusion to assess whether major aortopulmonary collateral arteries are providing adequate pulmonary artery blood flow [36].

Dual-Energy CT in Parenchymal Lung Disease

Congenital Lung Anomalies

PBV images can confirm the diagnosis and extent of congenital lung anomalies, such as congenital lobar overinflation, bronchial atresia, and congenital cystic adenomatoid malformation. Congenital lung anomalies show well-demarcated hypoperfusion relative to the adjacent lung [15] (Fig. 9). PBV images from dual-energy CT have shown feasibility in supplanting nuclear ventilation-perfusion (V/Q) scans in preoperative planning for resection of certain congenital lung lesions, for example in a small series showing excellent intermodality agreement for perfusion anomalies when coupled with a diagnostic-quality CT examination [19].

Chronic Lung Disease

Another use of PBV images is evaluation of the extent of parenchymal involvement in children with chronic lung disease. Chronic lung disease results in heterogeneous parenchymal perfusion, with the extent of heterogeneity varying with the severity of lung disease and associated pulmonary hypertension. The contributory effects of lung disease and pulmonary hypertension cannot be isolated on PBV images given that both entities can cause defects. Nonetheless, PBV images may show their summative effects and may have a role as a marker in subjectively grading the severity of chronic lung disease. Quantitative criteria have not been reported in the evaluation of chronic lung disease [19].

Dual-Energy CT in Oncology

Tumor Characterization

Dual-energy CT has shown utility in characterizing mediastinal masses on the basis of the iodine concentration in the tumor [17, 37]. Common mediastinal masses in children include lymphoma, teratoma, neurogenic tumors (neuroblastoma, ganglioneuroma, and neurofibroma), and foregut cysts. Mediastinal cysts typically have contents with an attenuation near that of water, but on occasion the attenuation may be higher, mimicking a solid mass, because the cyst fluid contains mucoid, protein, or blood products. Iodine images allow differentiation of solid and cystic masses based on the iodine concentrations. A non–iodine-containing mass is likely a cyst or benign solid mass, whereas an iodine-containing mass is more likely to be malignant (Fig. 10). Preliminary experience indicates that quantitative iodine concentrations greater than 1 mg/mL support the diagnosis of a malignant mass [17]. Dual-energy CT iodine images with subjective evaluation of iodine content can also be used to differentiate malignant and benign lung nodules [17].

Assessment of Treatment Response

Traditionally, assessment of treatment response has been based on reduction in tumor size over serial cross-sectional imaging examinations. However, tumors treated with immunotherapy may not show a size reduction but instead may reveal a change in attenuation. In this setting, iodine images derived from dual-energy CT can help to assess treatment response [17, 38]. Tumors with a poor response show a persistently high iodine concentration, whereas tumors that respond to treatment show a decrease in iodine content (Fig. 11). Currently, evaluation of treatment response is based on subjective evaluation of changes in iodine content. A quantitative decrease in iodine content using ROIs can support a diagnosis of treatment response. Large series in children that define response threshold values for decreased iodine content are lacking. Validation of threshold values will require future studies.

Pitfalls in Dual-Energy Imaging

Pitfalls in the diagnosis of pulmonary emboli on PBV images include beam-hardening artifact, errors in the dual-energy CT threshold, parenchymal disease, and physiologic cardiac motion, pleural motion, and diaphragmatic motion.

Beam-hardening artifacts resulting from dense contrast material in the superior vena cava and brachiocephalic vein cause areas of apparent underperfusion in the upper lobes [39] (Fig. 12). As previously noted, dual-source dual-energy CT uses maximum CT values to calculate pulmonary blood volume. In young children with dense lungs, the reference maximum attenuation is –200 to –300 HU, compared with a reference maximum attenuation of –600 HU in adolescents and adults; the reference minimum attenuation in both instances is set at –960 HU. Artifactual perfusion defects can occur in young children if an inappropriate adult setting is used [9, 40] (Fig. 12).

Other causes of artifactual perfusion defects are atelectasis, hemorrhage, and consolidation. These pathologies increase lung density and thus are assigned a value (expressed as Hounsfield units) that is outside the segmentation range (i.e., attenuation values greater than –300 HU in the dense lung setting or –600 HU in the adult lung setting). These artifacts are easily recognized by

viewing PBV images in combination with 70-kV, 80-kV, or mixed images [41, 42]. Motion artifacts related to cardiac contractions or inability to breath-hold cause characteristic crescentic perfusion defects adjacent to the heart, diaphragm, or pleura [43].

Conclusion

Dual-energy CT with material- and energy-specific imaging offers promising applications, previously unavailable with single-energy CT, for the evaluation of pediatric thoracic diseases. Material-specific imaging has increased the versatility of CT in the imaging of vascular and parenchymal abnormalities and has improved characterization of masses and assessment of therapy response. Virtual monoenergetic imaging has led to improvements in image contrast and has reduced beam-hardening artifacts. An especially important feature of dual-energy CT used in the evaluation of children is that the radiation exposure is comparable to or less than that of single-energy CT.

Provenance and review: Solicited; externally peer reviewed.

Peer reviewers: Gerald G. Behr, Memorial Sloan-Kettering Cancer Center; Jessie Aw, Ann & Robert H. Lurie Children's Hospital of Chicago; Robert J. Fleck, Cincinnati Children's Hospital Medical Center; additional individual(s) who chose not to disclose their identity.

References

1. Goo HW, Goo JM. Dual-energy CT: new horizon in medical imaging. *Korean J Radiol* 2017; 18:555–569
2. Johnson TRC. Dual-energy CT: general principles. *AJR* 2012; 199(suppl):S3–S8
3. McCollough CH, Leng S, Yu L, Fletcher JG. Dual- and multi-energy CT: principles, technical approaches, and clinical applications. *Radiology* 2015; 276:637–653
4. Patino M, Prochowski A, Agrawal MD, et al. Material separation using dual-energy CT: current and emerging applications. *RadioGraphics* 2016; 36:1087–1105
5. Siegel MJ, Kaza RK, Bolus DN, et al. White paper of the Society of Computed Body Tomography and Magnetic Resonance on dual-energy CT. Part 1. Technology and terminology. *J Comput Assist Tomogr* 2016; 40:841–845
6. Rassouli N, Etesami M, Dhanantwari A, Rajiah P. Detector-based spectral CT with a novel dual-layer technology: principles and applications. *Insights Imaging* 2017; 8:589–598
7. Almeida IP, Schyns LEJR, Öllers MC, et al. Dual-energy CT quantitative imaging: a comparison study between twin-beam and dual-source CT scanners. *Med Phys* 2017; 44:171–179
8. Euler A, Obmann MM, Szucs-Farkas Z, et al. Comparison of image quality and radiation dose between split-filter dual-energy images and single-energy images in single-source abdominal CT. *Eur Radiol* 2018; 28:3405–3412
9. Siegel MJ, Ramirez-Giraldo JC. Dual-energy CT in children: imaging algorithms and clinical applications. *Radiology* 2019; 291:286–297
10. Primak AN, Giraldo JCR, Eusemann CD, et al. Dual-source dual-energy CT with additional tin filtration: dose and image quality evaluation in phantoms and in vivo. *AJR* 2010; 195:1164–1174
11. Agostini A, Floridi C, Borgheresi A, et al. Proposal of a low-dose, long-pitch, dual-source chest CT protocol on third-generation dual-source CT using a tin filter for spectral shaping at 100 kVp for coronavirus disease 2019 (COVID-19) patients: a feasibility study. *Radiol Med (Torino)* 2020; 125:365–373
12. Gottumukkala RV, Kalra MK, Tabari A, Otrakji A, Gee MS. Advanced CT techniques for decreasing radiation dose, reducing sedation requirements, and optimizing image quality in children. *RadioGraphics* 2019; 39:709–726
13. Esquivel A, Ferrero A, Mileto A, et al. Photon-counting detector CT: key points radiologists should know. *Korean J Radiol* 2022; 23:854–865
14. Willemink MJ, Persson M, Pourmorteza A, Pelc NJ, Fleischmann D. Photon-counting CT: technical principles and clinical prospects. *Radiology* 2018; 289:293–312
15. Rapp JB, Biko DM, White AM, Ramirez-Suarez KI, Otero HJ. Spectral imaging in the pediatric chest: past, present and future. *Pediatr Radiol* 2022; 52:1910–1920
16. Meier A, Wurnig M, Desbiolles L, Leschka S, Frauenfelder T, Alkadhi H. Advanced virtual monoenergetic images: improving the contrast of dual-energy CT pulmonary angiography. *Clin Radiol* 2015; 70:1244–1251
17. Siegel MJ, Bhalla S, Cullinane M. Dual-energy CT material decomposition in pediatric thoracic oncology. *Radiol Imaging Cancer* 2021; 3:e200097
18. D'Angelo T, Cicero G, Mazziotti S, et al. Dual energy computed tomography virtual monoenergetic imaging: technique and clinical applications. *Br J Radiol* 2019; 92:20180546
19. Ramirez-Suarez KI, Barrera CA, Otero HJ, et al. Pilot study for comparative assessment of dual-energy CT and SPECT-CT V/Q scanning for lung perfusion evaluation in infants. *Pediatr Pulmonol* 2022; 57:702–710
20. Delesalle MA, Pontana F, Duhamel A, et al. Spectral optimization of chest CT angiography with reduced iodine load: experience in 80 patients evaluated with dual-source, dual-energy CT. *Radiology* 2013; 267:256–266
21. Bamberg F, Dierks A, Nikolaou K, Reiser MF, Becker CR, Johnson TRC. Metal artifact reduction by dual energy computed tomography using monoenergetic extrapolation. *Eur Radiol* 2011; 21:1424–1429
22. Siegel MJ, Curtis WA, Ramirez-Giraldo JC. Effects of dual-energy technique on radiation exposure and image quality in pediatric body CT. *AJR* 2016; 207:826–835
23. Zhang LJ, Wang ZJ, Zhou CS, Lu L, Luo S, Lu GM. Evaluation of pulmonary embolism in pediatric patients with nephrotic syndrome with dual energy CT pulmonary angiography. *Acad Radiol* 2012; 19:341–348
24. Goo HW. Dual-energy lung perfusion and ventilation CT in children. *Pediatr Radiol* 2013; 43:298–307
25. Lee EY, Tse SKS, Zurakowski D, et al. Children suspected of having pulmonary embolism: multidetector CT pulmonary angiography—thromboembolic risk factors and implications for appropriate use. *Radiology* 2012; 262:242–251
26. Barrera CA, Otero HJ, Fenlon EP 3rd, Francavilla ML, Ellison AM, Kaplan SL. CTA utilization for evaluation of suspected pulmonary embolism in a tertiary pediatric emergency department. *Clin Imaging* 2021; 75:105–110
27. Ikeda Y, Yoshimura N, Hori Y, et al. Analysis of decrease in lung perfusion blood volume with occlusive and non-occlusive pulmonary embolisms. *Eur J Radiol* 2014; 83:2260–2267
28. Kang MJ, Park CM, Lee CH, Goo JM, Lee HJ. Dual-energy CT: clinical applications in various pulmonary diseases. *RadioGraphics* 2010; 30:685–698
29. Lee CW, Seo JB, Song JW, et al. Evaluation of computer-aided detection and dual energy software in detection of peripheral pulmonary embolism on dual-energy pulmonary CT angiography. *Eur Radiol* 2011; 21:54–62
30. Otrakji A, Digumarthy SR, Lo Gullo R, Flores EJ, Shepard JAO, Kalra MK. Dual-energy CT: spectrum of thoracic abnormalities. *RadioGraphics* 2016; 36:38–52
31. Weidman EK, Plodkowski AJ, Halpenny DF, et al. Dual-energy CT angiography for detection of pulmonary emboli: incremental benefit of iodine maps. *Radiology* 2018; 289:546–553
32. Ameli-Renani S, Rahman F, Nair A, et al. Dual-energy CT for imaging of pulmonary hypertension: challenges and opportunities. *RadioGraphics* 2014; 34:1769–1790
33. Ascha M, Renapurkar RD, Tonelli AR. A review of imaging modalities in pulmonary hypertension. *Ann Thorac Med* 2017; 12:61–73
34. Shin SM, Kim HK, Crotty EJ, Hammill AM, Wusik K, Kim DH. CT angiography findings of pulmonary arteriovenous malformations in children and young

adults with hereditary hemorrhagic telangiectasia. *AJR* 2020; 214:1369–1376
35. Zucker EJ, Kino A, Schmiedeskamp H, Hinostroza V, Fleischmann D, Chan FP. Feasibility and utility of dual-energy chest CTA for preoperative planning in pediatric pulmonary artery reconstruction. *Int J Cardiovasc Imaging* 2019; 35:1473–1481
36. Schicchi N, Fogante M, Esposto Pirani P, et al. Third-generation dual-source dual-energy CT in pediatric congenital heart disease patients: state-of-the-art. *Radiol Med (Torino)* 2019; 124:1238–1252
37. Lee SH, Hur J, Kim YJ, Lee HJ, Hong YJ, Choi BW. Additional value of dual-energy CT to differentiate between benign and malignant mediastinal tumors: an initial experience. *Eur J Radiol* 2013; 82:2043–2049
38. Baxa J, Vondráková A, Matoušková T, et al. Dual-phase dual-energy CT in patients with lung cancer: assessment of the additional value of iodine quantification in lymph node therapy response. *Eur Radiol* 2014; 24:1981–1988
39. Kang MJ, Park CM, Lee CH, Goo JM, Lee HJ. Focal iodine defects on color-coded iodine perfusion maps of dual-energy pulmonary CT angiography images: a potential diagnostic pitfall. *AJR* 2010; 195:[web]W325–W330
40. Rapp JB, Biko DM, Barrera CA, Kaplan SL, Otero HJ. Current and future applications of thoracic dual-energy CT in children: pearls and pitfalls of technique and interpretation. *Semin Ultrasound CT MR* 2020; 41:433–441
41. Kim BH, Seo JB, Chae EJ, Lee HJ, Hwang HJ, Lim C. Analysis of perfusion defects by causes other than acute pulmonary thromboembolism on contrast-enhanced dual-energy CT in consecutive 537 patients. *Eur J Radiol* 2012; 81:e647–e652
42. Alis J, Latson LA Jr, Haramati LB, Shmukler A. Navigating the pulmonary perfusion map: dual-energy computed tomography in acute pulmonary embolism. *J Comput Assist Tomogr* 2018; 42:840–849
43. Rapp JB, Ho-Fung VM, Ramirez KI, White AM, Otero HJ, Biko DM. Dual-source computed tomography protocols for the pediatric chest: scan optimization techniques. *Pediatr Radiol* 2022; 11:1–12

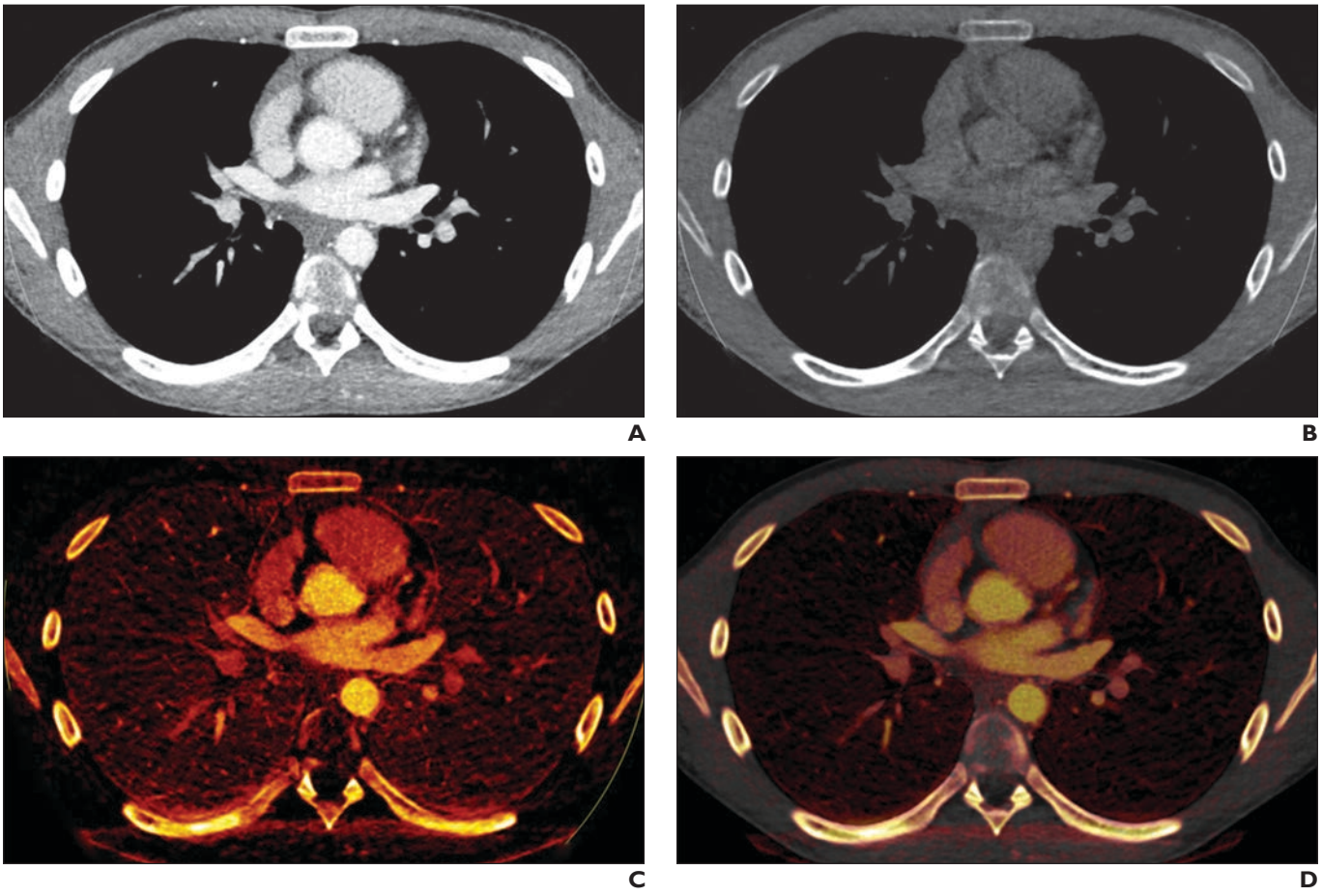

Fig. 1—Representative material-specific images from dual-energy CT examination performed to evaluate for metallic foreign body (not pictured) in 17-year-old boy.
A, Axial 100-keV image shows normal CT appearance with contrast.
B, Axial virtual unenhanced image created by subtraction of iodine content shows normal CT appearance with contrast removed.
C, Axial pure-iodine image shows pure contrast image with CT subtracted.
D, Axial iodine overlay image, which superimposes color-coded iodine map on gray-scale virtual unenhanced image, shows fused contrast and CT image.

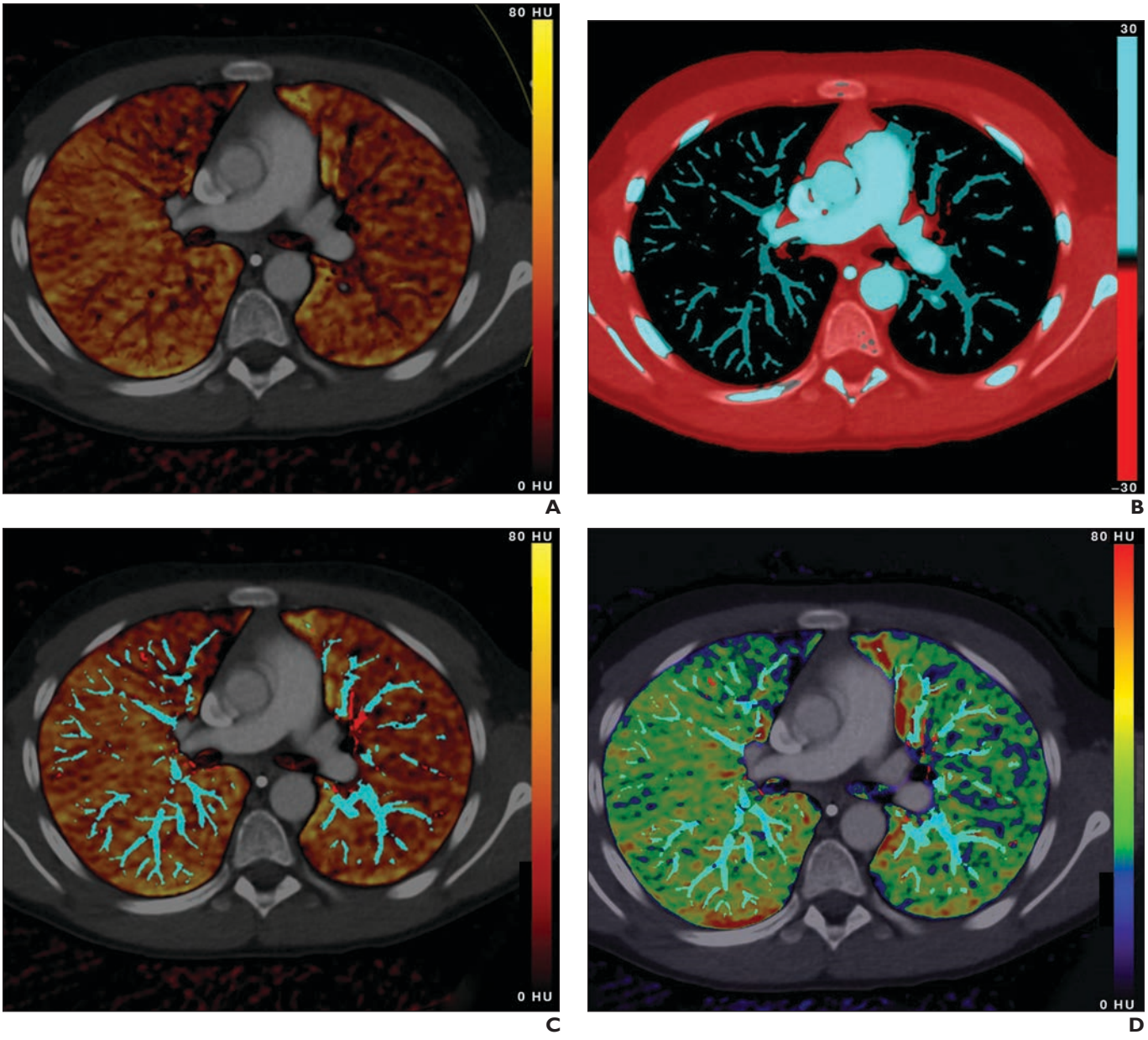

Fig. 2—Representative material-specific images from dual-energy CT examination performed to evaluate for pulmonary embolism in 11-year-old boy.
A, Standard axial perfused blood volume image shows good perfusion, color-coded reddish orange.
B, Axial pulmonary vessel image shows intravascular contrast, color-coded blue.
C, Axial perfused blood volume image with vessel overlay shows normal perfusion and intravascular contrast.
D, Multicolor perfused blood volume image (alternative to image in **C**) with vessel overlay shows good perfusion, color-coded green. Examination was interpreted as showing no pulmonary embolism or perfusion abnormalities.

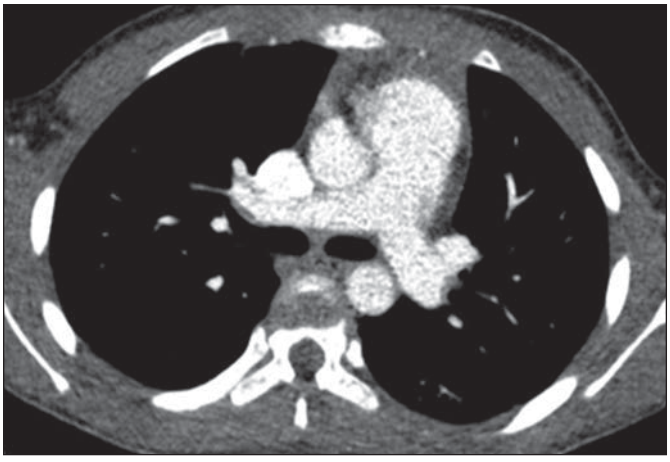

A

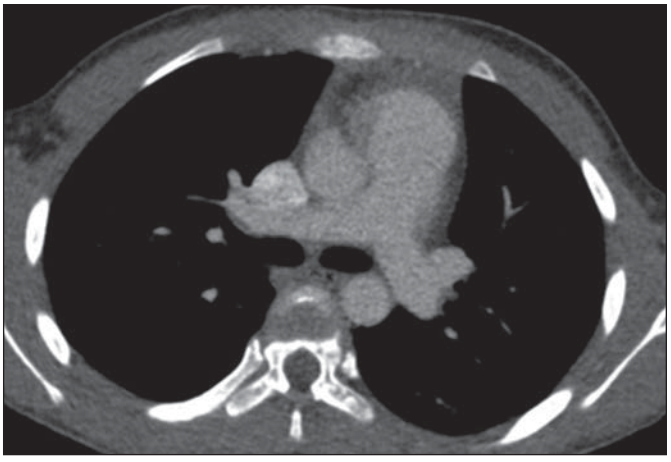

B

C

Fig. 3—Representative monoenergetic images, obtained using low kiloelectron voltage, from dual-energy CTA examination performed to evaluate for pulmonary embolism in 16-year-old boy with chest pain.
A–**C,** Axial 50- (**A**), 75- (**B**), and 100-keV (**C**) images show that visualization of iodine contrast improves at lower kiloelectron voltage. No pulmonary embolism was detected.

A

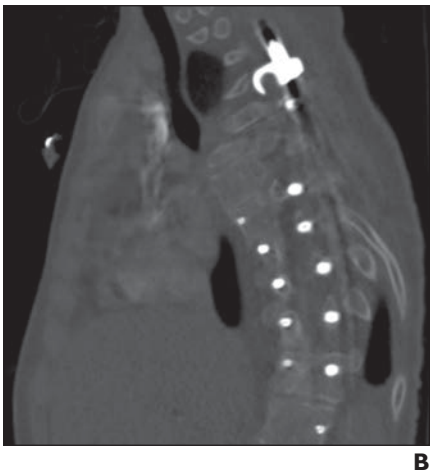

B

Fig. 4—Representative monoenergetic images used to suppress metal artifact from spinal instrumentation for scoliosis, from dual-energy CT examination performed in 13-year-old boy with back pain.
A and **B,** Sagittal 80- (**A**) and 180-keV (**B**) images show decreased beam-hardening artifact and improved visualization of posterior spinal hardware and surrounding structures at higher kiloelectron voltage. Conversely, soft-tissue contrast decreases with increasing kiloelectron voltage.

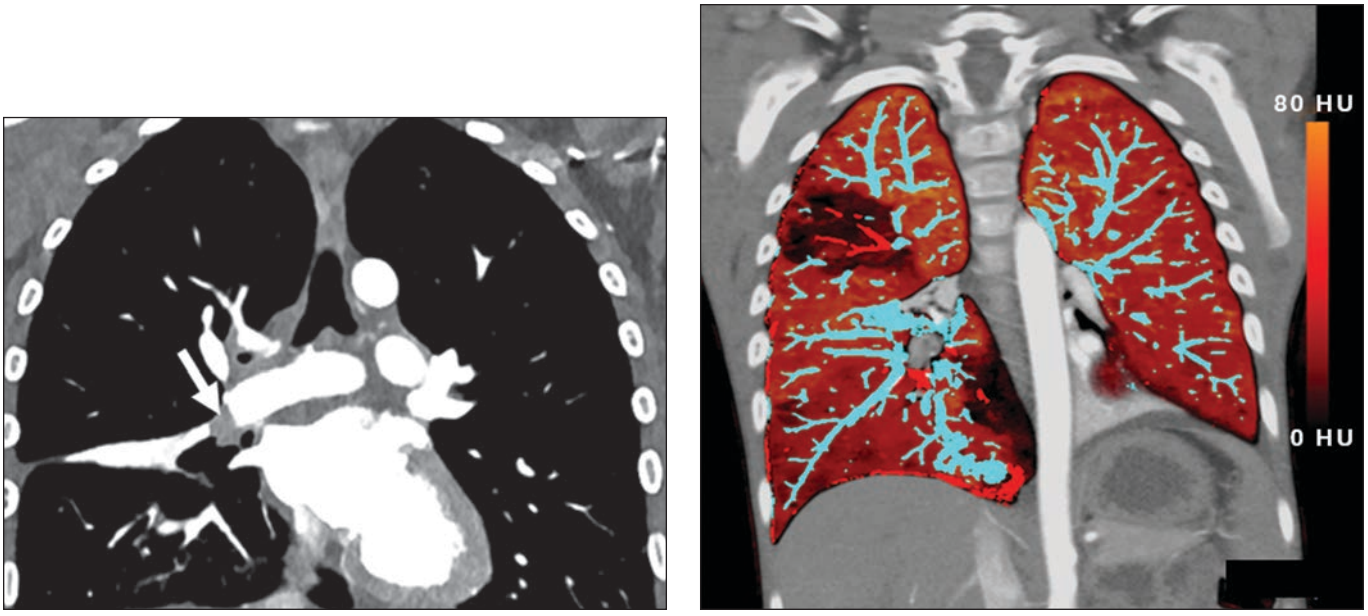

Fig. 5—5-year-old boy with acute respiratory distress. Dual-energy CTA was performed for further evaluation.
A, Coronal image shows thrombus in right pulmonary artery (*arrow*) and scattered areas of atelectasis in right lower lobe.
B, Coronal combined vessel and blood volume image shows wedge-shaped area of diminished perfusion (*black*) in right upper lobe, consistent with infarct. Right upper lobe vessels with diminished flow are color-coded red, and normal vessels in remainder of lung are color-coded blue. Color scale represents attenuation (expressed as Hounsfield units) of contrast media, which ranged from 80 HU (*orange*) to 0 HU (*black*). Higher numbers indicate better perfusion. Presence of contrast medium (CM) in vessels is shown, with less CM color-coded red and more CM color-coded blue.

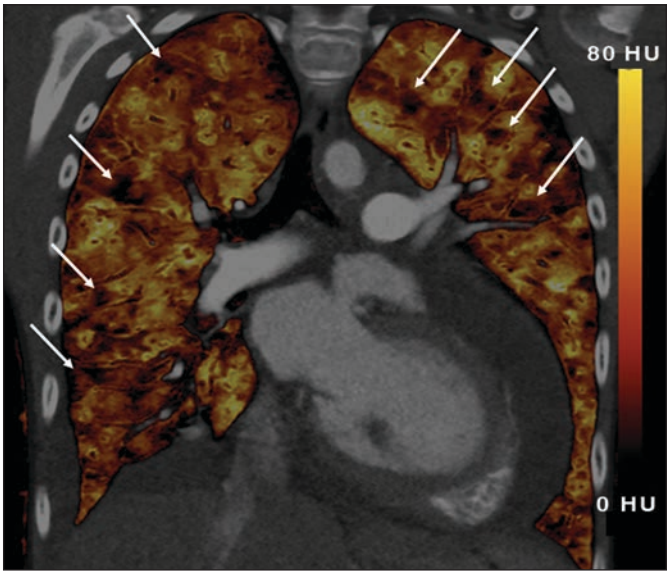

Fig. 6—13-year-old patient with primary pulmonary hypertension. Dual-energy CTA was performed for evaluation. Coronal perfused blood volume image shows multiple small, patchy, dark areas (*arrows*), consistent with nonsegmental perfusion defects; finding is typical of nonembolic pulmonary hypertension. Color scale represents attenuation (expressed as Hounsfield units) of contrast media, which ranged from 80 HU (*yellow*) to 0 HU (*black*).

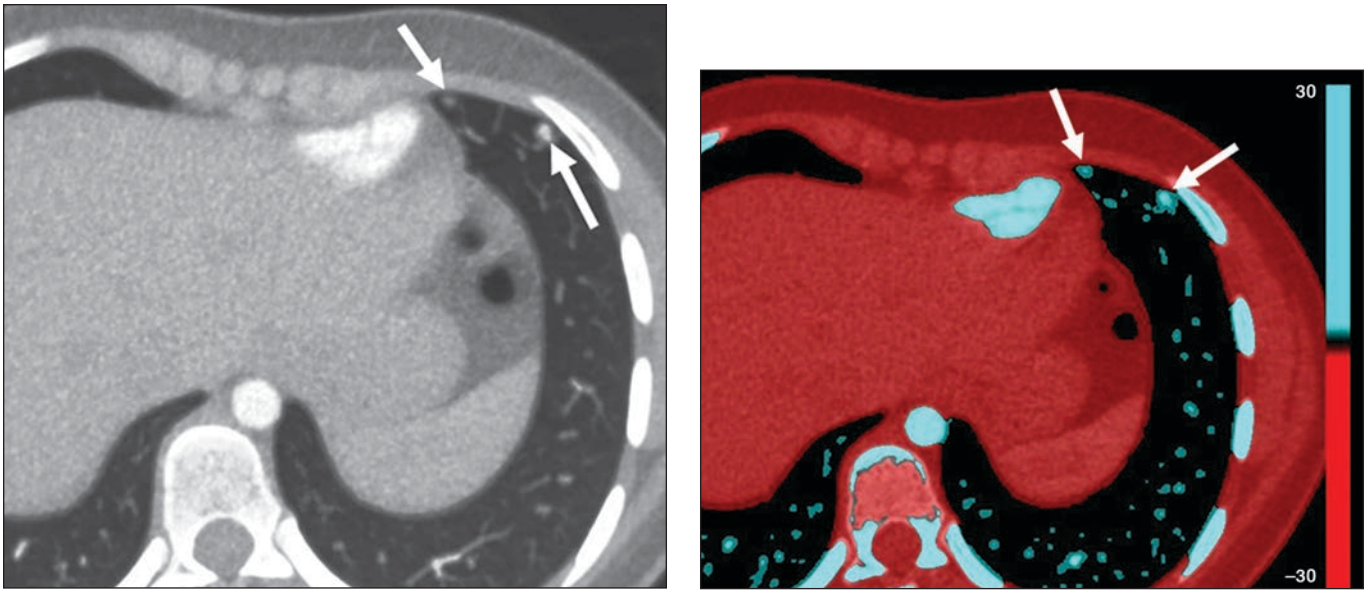

Fig. 7—14-year-old girl with hereditary hemorrhagic telangiectasia. Dual-energy CTA was performed for evaluation.
A, Axial maximum-intensity-projection image shows two small arteriovenous malformations in lingua of left upper lobe (*arrows*).
B, Axial blood-vessel image shows high-velocity flow, color-coded blue, in arteriovenous malformation (*arrows*). Blood vessel image increases conspicuity of malformation and may increase diagnostic confidence.

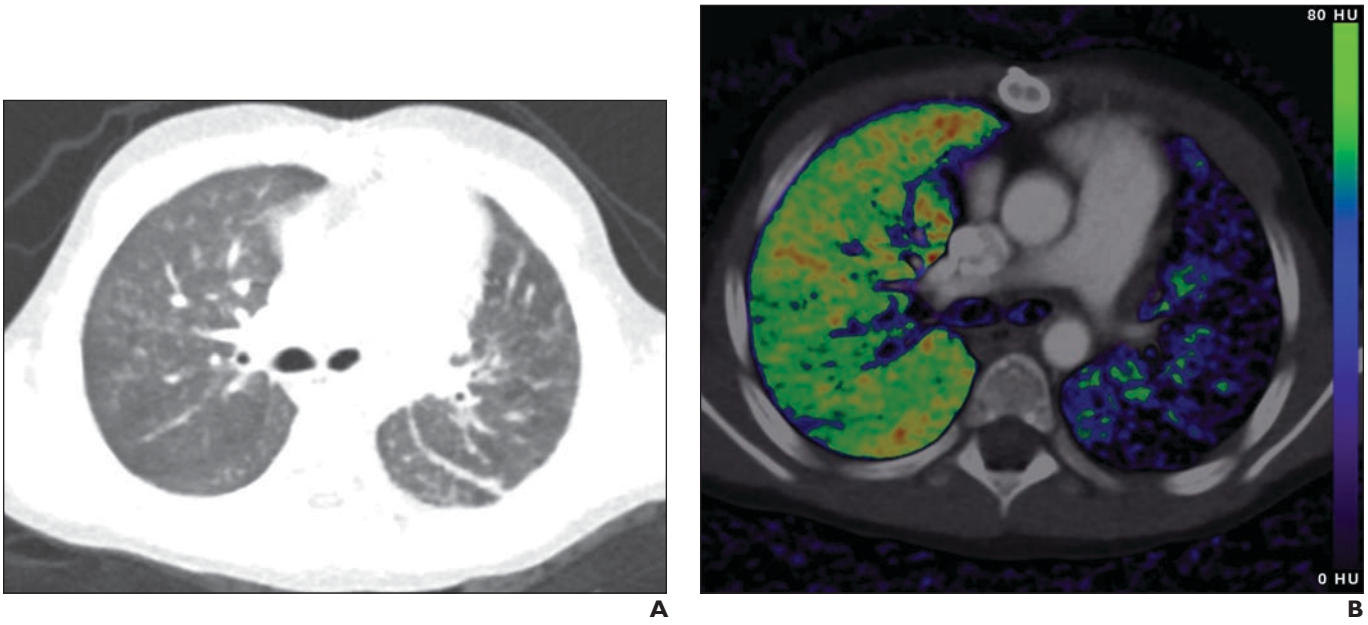

Fig. 8—5-year-old girl with pulmonary vein atresia in left upper lobe and pulmonary vein stenosis in left lower lobe. Dual-energy CT was performed for evaluation.
A, Axial image on lung window, obtained at 80 kV, shows small left lung with diminished vascularity.
B, Axial perfused blood volume image shows markedly diminished perfusion throughout left lung, color-coded blue. Normal perfusion is seen in right lung. Color scale represents attenuation (expressed as Hounsfield units) of contrast media, which ranged from 80 HU (*green*) to 0 HU (*black*).

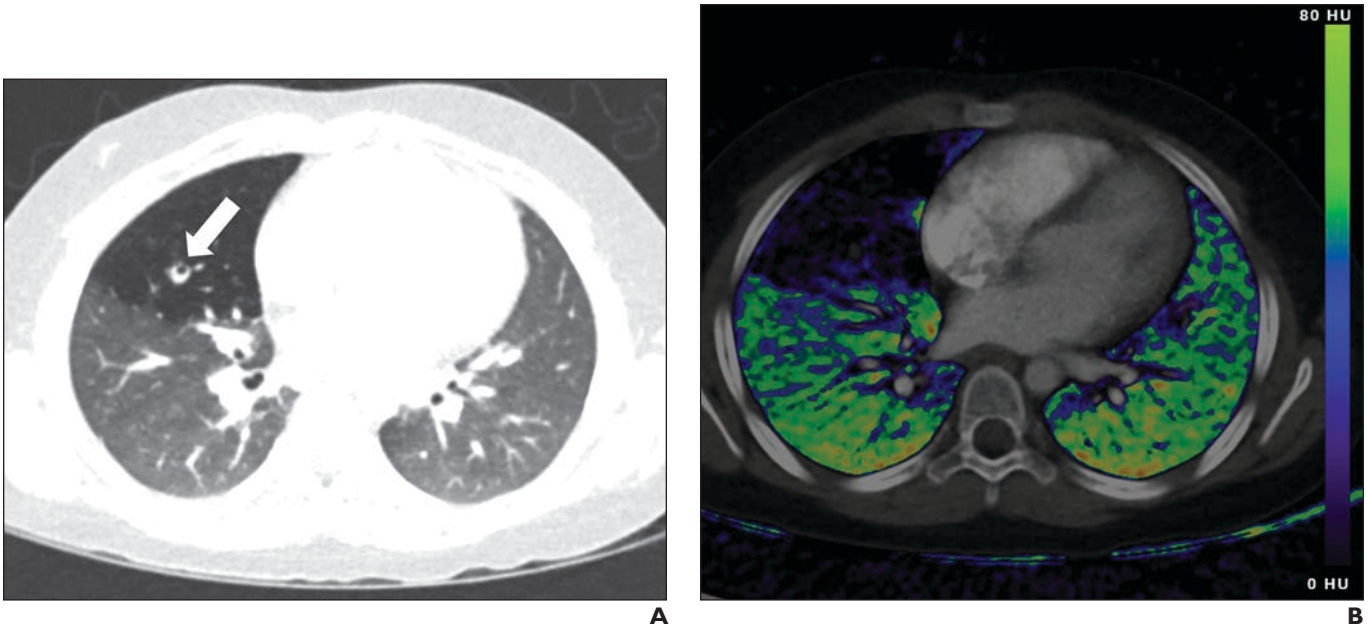

Fig. 9—8-year-old girl with congenital bronchial atresia. Dual-energy CT was performed for evaluation.
A, Axial image on lung window shows atretic bronchus (*arrow*) and surrounding hyperinflated lung in right upper lobe.
B, Axial perfused blood volume image shows corresponding hypoperfused right upper lobe, color-coded blue. Remainder of lung is normal.

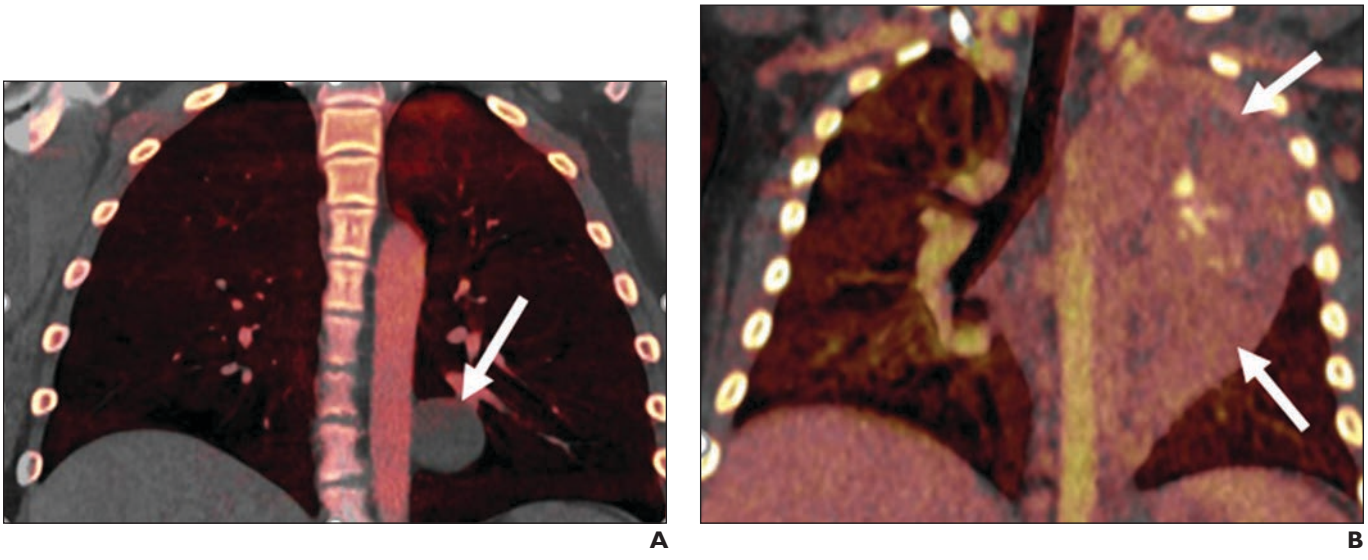

Fig. 10—Two patients who underwent dual-energy CT for evaluation of mediastinal masses.
A, Coronal iodine overlay image of 10-year-old boy shows no visualized iodine content in middle mediastinal mass (*arrow*). On conventional image (not shown), mass had attenuation of 40 HU, which was indeterminate for cyst. Iodine content measurement was 0.7 mg/mL, indicating presence of cystic mass. Surgical resection confirmed diagnosis of bronchogenic cyst.
B, Coronal iodine overlay image of 3-year-old boy shows iodine content within posterior mediastinal mass (*arrows*). Iodine content measurement was 3.2 mg/mL. Surgical resection confirmed diagnosis of neuroblastoma. Presence of iodine increases confidence in diagnosis of malignant mass. Mass containing iodine is more likely to be malignant than mass not containing iodine.

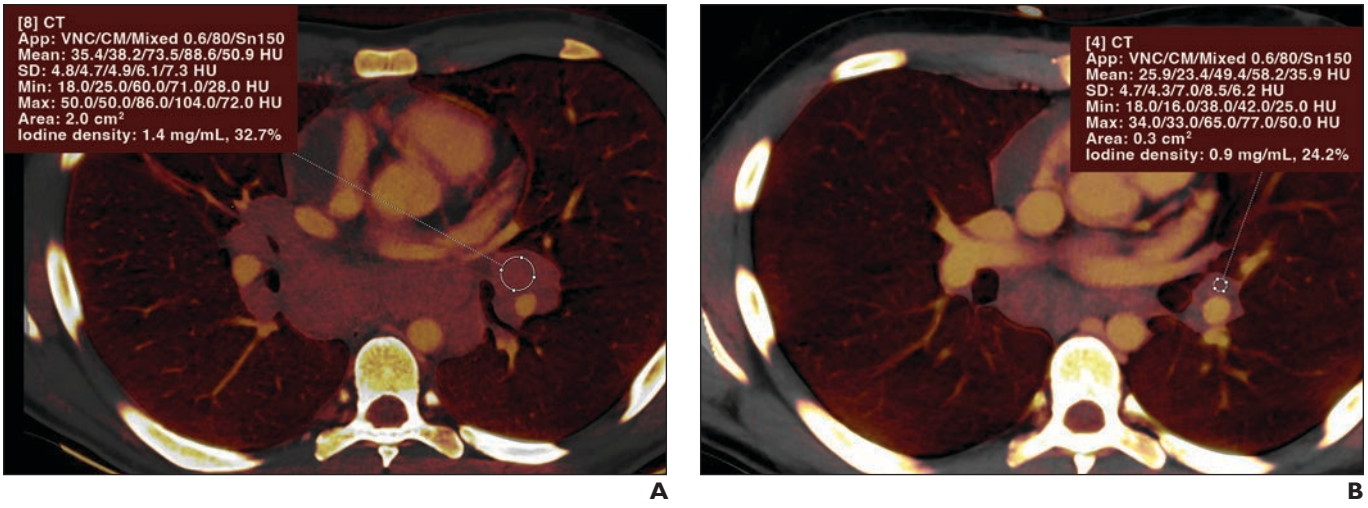

Fig. 11—16-year-old girl with lymphoma. Dual-energy CT was used to evaluate treatment response. App = application, VNC = virtual noncontrast, CM = contrast medium, Min = minimum, Max = maximum.
A, Axial iodine image from baseline examination shows iodine content in bilateral hilar and subcarinal lymph nodes. Iodine content in left hilar node measured by ROI (*circle*) was 1.4 mg/mL.
B, Axial iodine image from examination performed 6 weeks after treatment shows substantial decrease in size and iodine content of aforementioned lymph nodes, with residual patchy iodine content. Iodine content in left hilar node measured by ROI (*circle*) was 0.9 mg/mL. Findings are consistent with partial treatment response, which was confirmed by subsequent FDG PET/CT examination (not shown).

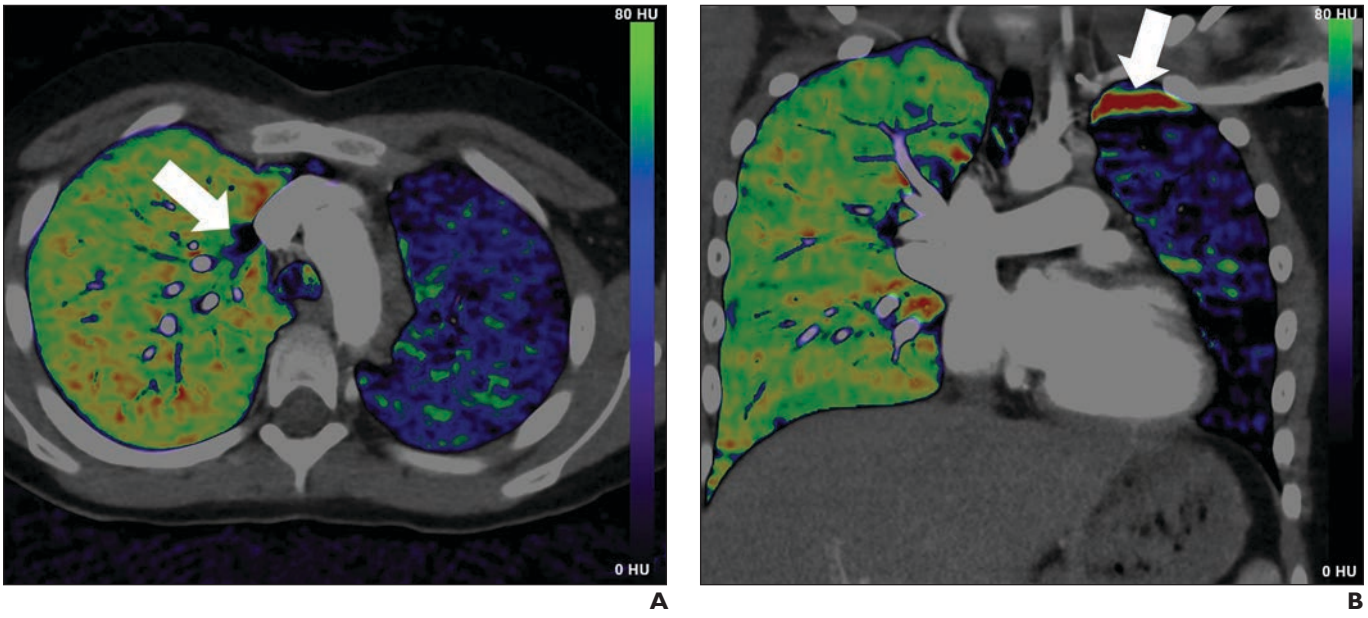

Fig. 12—Examples of potential pitfalls in application of dual-energy CT for evaluation of thorax in children.
A and **B,** Status of 7-year-old girl after repair of total anomalous pulmonary venous return. Dual-energy CT was performed for evaluation. Axial perfused blood volume map (**A**) shows focal area of apparent hypoperfusion (*arrow*), which was attributed to streak artifact from adjacent right brachiocephalic vein or superior vena cava. Coronal perfusion map (**B**) also shows focal area of apparent hyperperfusion (*arrow*), attributed to streak artifact from adjacent left brachiocephalic vein. True hypoperfusion is seen throughout left lung due to atresia of reimplanted pulmonary veins.

(Fig. 12 continues on next page)

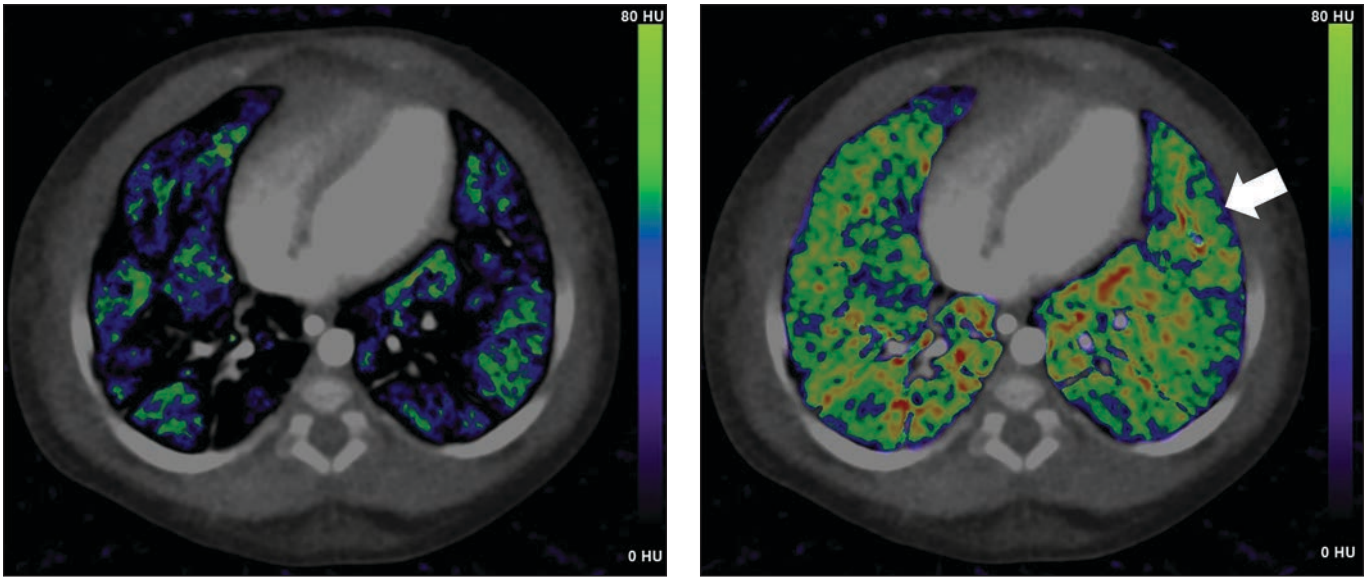

Fig. 12 (continued)—Examples of potential pitfalls in application of dual-energy CT for evaluation of thorax in children.
C and **D,** 5-month-old boy with bronchopulmonary dysplasia. Dual-energy CT was performed for evaluation. Axial perfused blood volume image (**C**) obtained without use of dense lung setting (maximum attenuation value cutoff set to –600 HU) shows heterogeneous parenchymal perfusion (*blue* and *black*), suggesting presence of multiple perfusion defects. Axial perfused blood volume image (**D**) at same level, generated with correct algorithm setting with use of dense lung setting, shows overall well-perfused parenchyma (*green*), aside from scattered small parenchymal perfusion defects (*blue*), consistent with underlying lung disease. Apparent perfusion defects in **C** were attributed to artifact. In **D**, area of surrounding lungs color-coded blue (*arrow*) relates to pleural motion from absence of breath-holding, representing additional artifact.

Editorial Comment: A Call for Pediatric Radiologists to Explore Dual-Energy CT

This article provides an excellent review of pediatric thoracic dual-energy CT (DECT), describing the technique and its utility as well as implicitly making a strong case for its expanded use.

Differences in x-ray energy absorption were routinely exploited before the advent of CT. A chest radiograph showing an opacity that might be calcium would be repeated at a lower peak kilovoltage setting, accentuating contrast as calcium's K-edge was approached. CT introduced the routine ability to distinguish a wide range of image contrasts. The wide dynamic range of CT images, however, did not fully resolve limitations from overlapping tissue attenuations. DECT addresses this issue, reviving an old concept.

As in adults, DECT has substantial potential benefit in children. Pediatric radiologists primarily use single-phase protocols for contrast-enhanced CT, leading to challenges in differentiating hyperattenuating structures from enhancing tissues. Virtual noncontrast images enable such differentiation. However, although DECT shows promise for pediatric indications, adoption of DECT by pediatric radiologists has been slow. Contributing to this limited adoption has been a need for further validation. For example, assessment of congenital lung disease, although promising, remains based on findings from small series. Although data supporting the use of iodine concentration thresholds for differentiating benign from malignant lesions are starting to accrue, such data must be expanded to a greater diversity of tumor types [1]. The further accumulation of evidence and experience in adults should spur a call for more studies in children [2]. Another issue is that although radiation doses for DECT are generally comparable to or lower than those for conventional CT, there are exceptions, such as for rapid-kilovoltage-switching scanners. In addition, dual-source scanners are somewhat prone to motion artifact, a particular concern in children [3].

Pediatric radiologists should recognize the potential benefits of DECT in children and should become active participants in advancing the technology through further clinical use and continued research into its most promising applications.

Gerald G. Behr, MD
Memorial Sloan Kettering Cancer Center
New York, NY
behrg@mskcc.org

Version of record: Aug 16, 2023

The author declares that there are no disclosures relevant to the subject matter of this article.

doi.org/10.2214/AJR.23.29658

Provenance and review: Solicited; not externally peer reviewed.

References

1. Siegel MJ, Bhalla S, Cullinane M. Dual-energy CT material decomposition in pediatric thoracic oncology. *Radiol Imaging Cancer* 2021; 3:e200097
2. Qian LJ, Zhu J, Zhuang ZG, et al. Differentiation of neoplastic from bland macroscopic portal vein thrombi using dual-energy spectral CT imaging: a pilot study. *Eur Radiol* 2012; 22:2178–2185
3. Kamps SE, Otjen JP, Stanescu AL, Mileto A, Lee EY, Phillips GS. Dual-energy CT of pediatric abdominal oncology imaging: private tour of new applications of CT technology. *AJR* 2020; 214:967–975